Ficus pandurata Hance suppresses colorectal cancer by targeting PI3K/Akt/mTOR pathway: A network pharmacology-guided experimental validation

Yuanyuan Luo
Guangdong Medical University
Bing Tang
Guangdong Medical University
Weibo Dai
Guangzhou University of Chinese Medicine
Yitong Chen
Guangdong Medical University
Hidayat Ullah
Guangdong Medical University
Weiwen Peng
Guangzhou University of Chinese Medicine
Yongdui Ruan
Guangdong Medical University
Xia Yuan
Guangdong Medical University
Weihong Kuang
Guangdong Medical University
Xianjing Hu
huxj2003@163.com
Guangdong Medical University

Research Article

Keywords: Ficus pandurata Hance, Colorectal cancer, PI3K/Akt/mTOR pathway, ATP limitation, Apoptosis, Network pharmacology

Posted Date: May 12th, 2025

DOI: https://doi.org/10.21203/rs.3.rs-6579300/v1

Additional Declarations: No competing interests reported.

Abstract

Background: *Ficus pandurata* Hance (FPH), a traditional Chinese medicinal herb, is known for its antioxidant and anti-inflammatory activities. While its efficacy against ulcerative colitis has been reported, its potential role in colorectal cancer (CRC) remains under explored. This study aimed to investigate the anti-CRC activity of FPH decoction (FPHD), focusing on its molecular targets and underlying mechanisms through an integrated approach of network pharmacology, molecular docking, and experimental validation.

Methods: The cytotoxicity of FPHD was assessed in CT-26 colorectal cancer cells and IEC-6 normal intestinal cells using the MTT assay. Anti-tumor efficacy was validated in a CT-26 tumor-bearing mouse model. Fifty-one bioactive compounds from FPHD were retrieved from prior UPLC-HRMS study. Potential targets were predicted via Swiss Target Prediction and PharmMapper, and intersected with CRC-related targets obtained from GeneCards, DisGeNET, Drug Bank, OMIM, and TTD databases. Network analysis, protein–protein interaction mapping, GO and KEGG enrichment, and molecular docking were conducted to identify core targets and pathways. Key findings were validated through Western Blot, ATP quantification, and flow cytometry.

Results: FPHD selectively suppressed CT-26 cell viability without harming IEC-6 cells and significantly reduced tumor volume in vivo. Network pharmacology identified 216 overlapping targets between FPHD and CRC, with enrichment pointing to the PI3K/Akt/mTOR pathway. Docking results showed strong binding affinity between major FPHD compounds and Akt1. Mechanistically, FPHD downregulated p-Akt and p-mTOR while upregulating LKB1 and p-AMPK, leading to reduced ATP production and caspase-dependent apoptosis in CRC cells.

Conclusion: This study reveals that FPHD exerts potent anti-tumor effects through modulation of the PI3K/Akt/mTOR axis, energy depletion, and apoptosis induction. These findings provide compelling evidence for the development of *Ficus pandurata*as a multi-target complementary therapeutic candidate for colorectal cancer management.

Background

Colorectal cancer (CRC) has emerged as a relentless global health burden—ranking among the top three causes of cancer-related deaths worldwide. It has shown a concerning upsurge in both incidence and mortality, particularly in rapidly developing nations like China (1). Despite aggressive advances in surgical techniques, chemotherapeutic regimens, and immunotherapies, the prognosis for many CRC patients remains poor, largely due to late-stage diagnosis, drug resistance, and systemic toxicity associated with conventional treatments (2, 3). This stark clinical reality underscores an urgent need for safer, multi-targeted, and biologically rational alternatives (4, 5). In this context, traditional Chinese medicine (TCM) has garnered renewed scientific interest as a reservoir of bioactive compounds with multi-target therapeutic potential, supported by centuries of empirical use and an expanding corpus of pharmacological and molecular evidence. Among these, *Ficus pandurata* Hance (FPH), an

ethnomedicinal herb native to southern China, holds untapped promise in oncological applications beyond its established anti-inflammatory and hepatoprotective roles.

Ficus pandurata, a traditional medicinal plant from the Moraceae family, has been historically used in southern China as a health-promoting soup, first documented in the Prescription of Jiangxi Folk Herbal Medicine. Rich in flavonoids, triterpenes, phenolic acids, and coumarins, FPH has demonstrated notable antioxidant, anti-inflammatory, and hepatoprotective effects in preclinical studies (6–9). Its aqueous root extract has been shown to reduce serum malondialdehyde (MDA) and elevate superoxide dismutase (SOD) levels, indicating potent free-radical scavenging activity (9). Our previous findings also revealed FPH's efficacy in alleviating ulcerative colitis through oxidative stress modulation—a condition closely linked to colorectal cancer development (10, 11). These data collectively highlight FPH as a promising candidate for further investigation in cancer therapeutics, although its precise anti-CRC mechanisms remain largely unexplored.

Given the multifactorial nature of colorectal cancer and the complexity of phytomedicines like FPH, a systems-level approach is essential to decode their therapeutic mechanisms. Network pharmacology, integrating bioinformatics, target prediction, and pathway enrichment, offers a powerful framework to dissect multi-component and multi-target interactions. When coupled with molecular docking and experimental validation, this approach provides mechanistic clarity and translational relevance (12, 13). Therefore, the present study aimed to systematically elucidate the anti-colorectal cancer mechanisms of *Ficus pandurata* Hance decoction (FPHD) by integrating network pharmacology, molecular docking, and experimental validation. Building upon previously characterized phytochemical profiles, we identified key bioactive compounds, predicted their therapeutic targets, and mapped associated signaling pathways, with a particular focus on the PI3K/Akt/mTOR axis. These computational findings were corroborated through in vitro cytotoxicity assays, in vivo tumor suppression models, and molecular analyses of apoptosis and energy metabolism. Through this multi-layered strategy, we sought to establish FPHD as a scientifically grounded, multi-target candidate for complementary CRC therapy.

Methods

Reagents and antibodies

5-FU (purity > 99.67%, HY-90006) was purchased from MedChemExpress (New Jersey, USA). Annexin V-FITC/PI double-stained cell apoptosis detection kit (BL110A) was obtained from Biosharp Technology Company (Hefei, China). An enhanced ATP detection kit (S0027) was procured from Beyotime Biotechnology Company (Shanghai, China). IL-2 (376210913) and IFN-γ (366210412) Elisa detection kits were provided by Tianjin Anoric Biotechnology Co., Ltd. (Tianjin, China). The primary antibodies against cleaved caspase 3 (9661S), p-AMPK (50081T), LKB1 (#3047), and Akt (#4685S) were supplied by Cell Signaling Technology Company (Beverly, MA, USA). The primary antibodies against β-actin (AF7018), cleaved PARP (AF7023), BAX (AF0083), Bcl-2 (AF6139), p-mTOR and (AF3308) were purchased from

Affinity Biosciences Ltd. (Cincinnati, OH, USA), and p-Akt (R22961) were acquired from ZEN-BIOSCIENCE (Chengdu, China).

Preparation of aqueous extraction of FPH

The FPH samples were collected from Dajin Village, Kaiping City, Guangdong Province, China, and authenticated by Prof. Huang Haibo from the Department of Identification, Guangzhou University of Traditional Chinese Medicine. Decoction preparation followed our previously reported method (6).

Cell culture

The CT-26 WT cells and IEC-6 cells were purchased from the Cell Resource Center, Shanghai Institute of Biological Sciences, Chinese Academy of Sciences. CT-26 WT cells were cultured in RPMI-1640 (Gibco, USA) and IEC-6 cells were cultured in DMEM (Meilun, Dalian, China) medium containing 10% fetal bovine serum. Cells were incubated at 37°C in a humidified atmosphere containing 5% CO_2.

Cells morphological observation

CT-26 and IEC-6 cells were planted in six-well plates at a cell density of 1×10^5 cells/well. After 24 h incubation, cells were treated with different concentrations of FPHD for 48 h. The cell morphology was observed and captured using an inverted fluorescence microscope.

Determination of cell viability

The cell viability was detected by 3-(4,5-dimethyl-2-thizolyl)-2,5-diphenyl-2H-tetrazolium bromide (MTT) assay. Briefly, CT-26 and IEC-6 cells at 3×10^3 cells/well were seeded in 96-well plates and grew in an incubator overnight. After cells were treated with different concentrations of FPHD for 48 h, 20 μL of MTT solution (5 mg/mL) was added and incubated for another 4 hours. After the supernatant being removed, 150 μL of DMSO was added to each well to dissolve the formazan. The absorbance value of each well was determined at 570 nm in a microplate reader.

In vivo xenograft experiment

Forty SPF-grade BALB/c mice (♂, 6–8 weeks old) were purchased from Guangdong Medical Experimental Animal Center, with laboratory animal license number SCXK (Guangdong) 2018-0002, and raised in Zhongshan Hospital of the Experimental Room of Traditional Chinese Medicine Pharmacology SPF animal room, with the license number of SYXK (Guangdong) 2020 – 2019. The mice were kept in a controlled environment with 12 hours of light and darkness, at a temperature of 22°C in the SPF facility. The animal experiment procedures were carried out strictly under the "Animal Guidelines for Ethical Review of Animal Welfare" (GB/T 35892–1272018) conducted by the laboratory and approved by the

Laboratory Animal Management and Ethics Committee of Guangzhou University of Traditional Chinese Medicine.

The density of CT-26 cells was adjusted to 5×10^6 cells/mL with 0.1 mL/mouse inoculated on the right flanks of the mice. When the tumor volume grew to 60 ~ 70 mm^3, the mice were randomly divided into five groups (each group with 8 mice) according to their body weight and tumor volume, including the normal group (no tumor mice), model group, 5-FU group (15 mg/kg), FPH low-dose group (200 mg/kg), and FPHD high-dose group (400 mg/kg). All drugs were given orally at a volume of 0.1 mL/10 g per dose. The administration continued for ten days, with daily monitoring of body weight and tumor volume in the mice throughout the treatment period (tumor volume = $1/2 \times W \times L^2$). Blood was collected 24 hours after the last treatment, and the tumor tissues, spleen, and thymus were collected and weighed. The spleen and thymus index were calculated using the following formula: immune organ index = immune organ mass (mg) / mouse body mass (g).

Enzyme-linked immunosorbent assay (ELISA)

Serum was obtained by centrifugation at 4°C and 10,000 rpm for 15 minutes. The concentrations of IL-2 and IFN-γ were measured using Elisa kits according to manufacturers' instructions (14).

Collection of active targets in FPHD

The chemical components in FPHD were identified in our previous study (9). The associated targets of chemical compounds in FPHD were retrieved from the Swiss Target Prediction database and PharmMapper database.

CRC-associated therapeutic targets

Therapeutic targets for CRC were obtained from the GeneCards database (https://www.genecards.org//), DrugBank database (https://www.drugbank.com), DisGeNET database (https://www.disgenet.org/), and OMIM database (https://www.omim.org/).

Network analysis

To investigate the potential mechanism of FPHD on CRC, the online tool of Venn (http://bioinfogp.cnb.csic.es/tools/venny/) was applied to draw a diagram to depict the relationship between FPHD and CRC. Whereafter, the overlapped targets of FPHD and CRC were imported into the STRING12.0 database (https://string-db.org) to construct a network of protein-protein interaction (PPI). “Homo sapiens” was selected as the condition of screening criterion for the organism, and the confidence score was set to be more than 0.4. Cytoscape3.7.2 (https://www.cytoscape.org/) was used to establish a PPI network and perform a topological and cluster analysis. Network parameters were calculated using Network Analyzer.

Functional enrichment analysis

The common targets of "FPHD-CRC" were assessed through Gene Ontology (GO) and Kyoto Encyclopedia of Genes and Genomes (KEGG) analyses. R packages, including clusterProfiler, org.Hs.eg.db, enrichplot, ggplot2, and DOSE packages, were utilized for the analysis process. The top ten GO terms were selected for visual representation of the analysis results. Bar charts were used to display the top twenty KEGG terms. The P-value and False Discovery Rate (FDR) were utilized to assess the correlation between FPHD and CRC.

Molecular docking

The SDF format files of compounds were downloaded from the PubChem database. The MM2 module of ChemDraw 3D was utilized for energy minimization to obtain the lowest energy conformation and saved as a mol2 file. The protein structures were downloaded from the UniProt database and visualized using PyMOL. Thereafter, operations such as dehydration, hydrogenation, charge calculation, and combination of non-polar hydrogen on the ligand and receptor were conducted through MgTools 1.5.6, and they were respectively saved in the pdbqt format. Finally, molecular docking between the ligand and receptor was performed using AutoDock Vina 1.1.2, and the docking results were visually displayed via PyMOL.

Western Blot

The CT-26 tumor tissue samples were homogenized with RIPA lysis buffer containing protease inhibitor and phosphatase inhibitor (Beyotime, Shanghai, China), and centrifuged at 4°C, 12,000 rpm for 10 minutes. Protein concentrations were measured using the BCA detection kit (Beyotime, Shanghai, China). Subsequently, the same amount of protein was electrophoresed on SDS-PAGE gel. The gels were transferred into PVDF membranes for 1–2 h, and the membranes were blocked with fast blocking solution for 15 min. The membrane was then washed with PBST three times, and incubated with the primary antibody of the target protein at 4°C overnight. The membranes were washed and incubated with the secondary antibody (1:10000) for 2 h at room temperature, and then the membranes were washed with PBST three times. An ECL Western Blot detection kit (Meilun, Dalian, China) was used to visualize the expression of the target protein, and Image J software was used to analyze the protein levels quantitatively (n = 3).

ATP detection

CT-26 cells at a density of 1×10^5 cells/well were seeded in a six-well plate. After incubation for 24 h, cells were treated with different concentrations of FPHD for 48 hours and then lysed with ATP lysis buffer. For the ATP detection in tumors, 20 mg of tumor tissues were obtained from CT-26 tumor-bearing mice, ATP lysis buffer at a ratio of 10:1 (V/W) was added, and ground at 4°C. After being lysed, cells were centrifuged at 12000 g, 4°C for 5 minutes and the supernatant was taken to evaluate the ATP concentration in accordance to the guidelines provided by the manufacturer. The ATP concentration was converted to nanomoles per milligram of protein. The normal group or the model group was used as a standard for statistical analysis for all groups.

Flow cytometry

CT-26 cells were dispensed into a six-well plate at a cell density of 1×10^5 cells/well. After incubating for 24 h, cells were treated with FPHD for 48 h. The cells were collected and then stained with Annexin-V FITC and PI according to the instructions of the Biosharp Apoptosis Kit.

Statistical analysis

At least three independent tests were performed for all assay conditions. All data was presented as means ± SEM. The statistical analysis was performed using one-way ANOVA for comparison between multiple groups, followed by Student's t-test for pairwise comparisons. All analyses were conducted using GraphPad Prism 8.0, and a p-value of less than 0.05 was considered statistically significant.

Results

FPHD suppressed colorectal cancer growth *in vitro* and *in vivo*

To assess the anti-tumor potential of FPHD, CT-26 colorectal cancer cells and IEC-6 normal intestinal epithelial cells were treated with FPHD for 48 hours. FPHD inhibited CT-26 cells proliferation in a dose-dependent manner while exhibiting no cytotoxicity toward IEC-6 cells, as confirmed by morphological observation and viability assays (Fig. 1A–B).

In vivo, FPHD significantly reduced tumor volume and tumor weight in CT-26 tumor-bearing mice (Fig. 2B–D) without affecting body weight, in contrast to 5-FU, which induced weight loss (Fig. 2A). These findings suggest that FPHD exerts anti-tumor effects with minimal systemic toxicity. The spleen and thymus are important immune organs in the human body, directly related to immune cells' growth, proliferation, and maturation. Compared to the 5-FU group, the spleen and thymus index of FPHD-treated groups significantly increased, indicating that FPHD protected the spleen and thymus from injury of mice (Fig. 2E and F). Next, we explored the effect of strengthening the tumor immunity on the response to FPHD therapy. We used the ELISA kits to detect IL-2 and IFN-γ levels in mouse serum. Compared to the control group, serum levels of IL-2 and IFN-γ were reduced in the model group, while they were significantly elevated in the FPHD-treated groups (Fig. 2G and H). Altogether, these results showed that FPHD significantly inhibited colorectal cancer growth *in vitro* and *in vivo.*

Network pharmacological analysis

Construction of a network linking drug ingredients and targets for FPHD in the management of CRC

A total of 51 active chemical compounds in FPHD were screened using the intersection of results from UPLC-HRMS (9). The chemical structures, OB (oral bioavailability, %), and DL (drug-likeness, score) information of the 51 compounds are presented in Table 1 (at the end of the document). The putative targets of these core compounds were predicted by Swiss Target

Prediction database and PharmMapper database, resulting in 1277 potential targets. Additionally, 1432 therapeutic targets for CRC treatment were obtained from multiple databases, including GeneCards, DrugBank, DisGeNET, TTD database, and OMIM database (Fig. 3A). A Venn diagram was generated to identify the potential targets of FPHD against CRC, revealing 216 common targets (Fig. 3B). Subsequently, the PPI network diagram analysis based on STRING showed that there were 216 nodes with an average node degree of 4.56 and a total of 493 edges in the target interaction network (Fig. 3D-F).

Herb-compound-pathway-target network analysis

The yellow circle nodes represent compounds in FPH, the red rhombus nodes represent the traditional Chinese medicine FPH, and the green quadrilateral represents the target of action and the edges denote the interactions between compounds and their respective targets (Fig. 4). This result implies that the FPH works synergistically through multiple components, multiple targets to treat CRC.

GO and KEGG analyses

CytoHubba was used to analyze overlapped genes in the PPI network. The top 30 genes by degree value in the PPI network were shown in Fig. 5A, and the top 5 genes were proto-oncogene tyrosine-protein kinase Src (SRC), RAC-alpha serine/threonine-protein kinase 1 (Akt1), catenin beta-1 (CTNNB1), epidermal growth factor receptor (EGFR) and estrogen receptor 1 (ESR1).

The underlying mechanisms of the core targets were analyzed through GO and KEGG pathway analyses. The findings of biological process (BP) indicated a significant correlation between the intersected genes and the process of apoptosis, highlighting its importance in the therapeutic effects of FPHD in CRC (Fig. 5B). The cellular component (CC) category mostly included cytosol, cytoplasm, receptor complex, etc. (Fig. 5B). Regarding molecular function (MF), FPHD primarily produced its effects through protein serine/threonine/tyrosine kinase activity and protein kinase activity (Fig. 5B). Additionally, KEGG pathway enrichment analysis identified 20 most representative entries, among which the PI3K-Akt signaling pathway is the most highly enriched (Fig. 5C).

Molecular docking analysis

To further elucidate the interactions between the main compounds (Sanleng acid, 4-Hydroxybenzoic acid, 7-Hydroxycoumarin, Succinic acid, Pyroracemic acid, trans-Aconitic acid, Protocatechuic acid, Methyl-5,7-dihydroxy-2(Z)-octenoate, 6-Gingerol, and Methyl(2,4-dihydroxy-3-formyl-6-methoxy) (phenylketone) in FPHD and top 3 key targets (SRC, Akt1, and CTNNB1), we conducted the molecular docking analysis using AutoDock. The absolute value of the binding energy is higher, indicating stronger affinity and stability between the components and the target. Generally, an absolute value greater than 5.0 indicates good binding activity, while an absolute value surpassing 7.0 signifies strong binding activity

Table 2
The binding energy between compounds and targets.

No.			Molecular name	Affinity (Kcal/mol)		
				SRC	Akt1	CTNNB
1	Sanleng acid	-5.8	-6.8	-4.6		
2	4-Hydroxybenzoic acid	-5.2	-5.8	-4.8		
3	7-Hydroxycoumarin	-6.1	-7	-5.6		
4	Succinic acid	-4	-4.5	-4.2		
5	Pyroracemic acid	-3.6	-3.9	-3.5		
6	trans-Aconitic acid	-5.1	-5.4	-4.9		
7	Protocatechuic acid	-5.2	-6.3	-5		
8	Methyl-5,7-dihydroxy-2(Z)-octenoate	-5.1	-5.4	-4.4		
9	6-Gingerol	-6.2	-7.4	-4.3		
10		Methyl(2,4-dihydroxy-3-formyl-6-methoxy)phenylketone	-5.8	-6.1	-3.9	

between the component and its corresponding target. As shown in Table 2, the 10 main compounds have good binding affinity with Akt1 protein, among which gingerol has the strongest binding ability. The PyMoL software was used to visualize the target protein binding with small molecules (Fig. 6). The docking results showed that hydrophobic interactions, especially hydrogen bonds, mainly mediate the binding between the compounds and the target proteins.

FPHD suppressed CRC growth via limiting ATP production by regulating the PI3K/Akt/mTOR signaling pathway

According to the findings from the KEGG analysis, the PI3K-Akt signaling pathway showed the strongest association with FPHD-treated CRC. To further elucidate the underlying mechanism, the effect of FPHD on the PI3K/Akt/mTOR signaling pathway, which plays a key role in regulating cell apoptosis and energy metabolism, was assessed. As depicted in Fig. 7A-E, the expression of LKB1 and p-AMPK was increased under FPHD exposure, while the phosphorylation of Akt and mTOR was decreased. Next, the relative ATP levels in tumor tissues and CRC cells were subsequently measured. As shown in Fig. 7F, the ATP levels in tumor tissues of FPHD groups were significantly decreased compared to the model group ($p < 0.01$). In addition, FPHD dose-dependently decreased the level of ATP in CRC cells (Fig. 7G), suggesting that

FPHD suppressed CRC growth by limiting energy production. Altogether, these results indicated that FPHD limited the energy production of CRC by modulating the PI3K/Akt/mTOR signaling pathway.

FPHD inhibited CRC cell growth via inducing apoptosis

Akt is the primary regulator of cell survival, exerting its effects by directly inhibiting pro-apoptotic proteins or suppressing pro-apoptotic signals generated by transcription factors. To determine whether FPHD induced apoptosis in tumor tissue, protein expression levels in the tumor tissues were assessed using Western blot analysis. The results showed that FPHD up-regulated the relative protein expression levels of cleaved PARP, cleaved caspase 3, and the ratio of BAX/Bcl-2 (Fig. 8A-D). Flow cytometry was utilized to identify apoptosis using Annexin V and PI staining *in vitro*. The apoptosis ratio was significantly increased in a dose-dependent manner in CRC cells (Fig. 8E-F). Furthermore, Z-VAD-fmk, a pan-caspase inhibitor, significantly reduced the apoptosis induction of FPHD on CT-26 cells, suggesting that FPHD caused CRC apoptosis in a caspase-dependent manner (Fig. 8H-G). These data demonstrate that FPHD inhibits CRC growth by inducing apoptosis both *in vivo* and *in vitro*.

Discussion

With the persistent limitations of conventional colorectal cancer therapies—marked by systemic toxicity, resistance, and incomplete efficacy, complementary and alternative medicines are no longer optional adjuncts, but emerging as indispensable components in the search for safer, multi-targeted, and biologically integrative treatment strategies (15). In this context, *Ficus pandurata* Hance (FPH), a traditional medicinal plant long used in southern China, has attracted growing attention due to its antioxidant, anti-inflammatory, and hepatoprotective effects (9). Our previous findings demonstrated that FPH alleviates ulcerative colitis, a condition intricately linked to colorectal carcinogenesis, suggesting its broader therapeutic relevance. As a medicinal resource in Guangdong traditional healthcare materials have shown promising responses in preclinical tumor models and patients, offering potential for CRC treatment (16, 17). Traditional Chinese medicines target multiple pathways and biological processes while exhibiting lower toxicity compared to conventional treatments (18–21). The compounds found in FPHD are known to exhibit various bioactivities, including anti-inflammatory, antioxidant, and hepatoprotective effects (6, 9, 22). In this study, FPHD was shown to inhibit the CRC cells *in vivo* and *in vitro*, indicating FPHD as a novel treatment for CRC. However, due to the complexity of traditional Chinese medicine, fully elucidating the mechanisms by which FPHD treats CRC using conventional pharmacological methods remains challenging. Therefore, this study utilized a network pharmacology approach to systematically explore the underlying mechanisms of FPHD in the treatment of CRC. To address this, we adopted a network pharmacology-guided strategy, supported by molecular docking and experimental validation, to decode the multi-component and multi-target nature of FPH decoction (FPHD). Fifty-one bioactive compounds were computationally linked to 1,277 predicted targets, of which 216 overlapped with colorectal cancer-related genes. Functional enrichment highlighted the PI3K/Akt/mTOR signaling pathway, a key axis in tumor cell growth, metabolism, and survival, as the central node of FPHD action.

PI3K/Akt/mTOR signaling pathway plays a vital role in cell metabolism and growth. It has been found that targeting the PI3K/Akt/mTOR signaling pathway is a potentially effective way of treating cancer. LKB1 is an important serine/threonine kinase, and LKB1 could phosphorylate and activate AMPK (23). Akt could directly phosphorylate and inactivate TSC2, resulting in an activation of mTOR (24). Additionally, mTOR could be inhibited by AMPK via the phosphorylation of the of the phosphorylation of TSC2 (25). According to network analysis, FPHD might inhibit CRC growth by regulating the PI3k/Akt/mTOR signaling pathway. The relative protein expression of the PI3k/Akt/mTOR signaling pathway was detected to proceed with Western Blot and immunochemistry staining. The data indicated that FPHD was capable of up-regulating the LKB1 and p-AMPK protein expression and down-regulating the phosphorylation expression of Akt and mTOR protein. In our present study, FPHD could inhibit the PI3K/Akt/mTOR signaling pathway, leading to limiting ATP production and affecting the cellular energy homeostasis of CRC cells. It suggested that FPHD suppressed CRC cell growth by regulating the PI3K/Akt/mTOR signaling pathway.

Apoptosis is a crucial pathway that regulates cell death, marked by chromatin condensation, nuclear and cell fragmentation, and the development of apoptotic bodies (26). The core apoptotic signaling pathways include the intrinsic way and the extrinsic way. Prior studies have indicated a connection between apoptosis and tumors, particularly in the development of colorectal cancer and the ability to resist chemotherapy medications (27). Therefore, some approved anti-cancer drugs directly regulate the apoptosis pathway, and targeting the apoptosis pathway is a promising anti-tumor strategy (28). Our study revealed that the GO enrichment analysis of BP results indicated a significant impact of FPHD on apoptosis. We further investigated the impact of FPHD treatment on apoptosis in CRC cells. Cleaved caspase 3 and cleaved PARP are molecular biomarkers of apoptosis. Moreover, in the apoptosis pathway, the Bcl-2 protein inhibits apoptosis, while the BAX protein promotes apoptosis. Our research investigated the expression of proteins related to apoptosis in CRC cells treated with FPHD. The findings indicated a rise in cleaved PARP and an elevation in the BAX/Bcl-2 ratio. These results demonstrate that FPHD up-regulated apoptosis-related proteins and activated apoptosis pathways in CRC cells, suggesting that FPHD inhibits CRC cell growth by regulating apoptosis.

Conclusions

This study provides compelling evidence that *Ficus pandurata* Hance decoction (FPHD) exerts potent anti-colorectal cancer effects through a multifaceted mechanism involving inhibition of the PI3K/Akt/mTOR signaling pathway, disruption of cellular energy metabolism, and induction of caspase-dependent apoptosis. By integrating network pharmacology, molecular docking, and experimental validation, we identified Akt1 as a central target of key FPHD compounds and confirmed that modulation of this pathway results in significant tumor growth suppression *in vitro* and *in vivo*. Additionally, FPHD preserved immune organ function and restored cytokine levels, further supporting its therapeutic relevance. These findings establish FPHD as a promising complementary candidate in colorectal cancer management, offering a mechanistically grounded, multi-target alternative to conventional

monotherapies. Future clinical studies are warranted to translate these preclinical insights into practical oncological applications.

Abbreviations

FPH	*Ficus pandurata* Hance
CRC	Colorectal cancer
FPHD	*Ficus pandurata* Hance detection
GO	Gene ontology
KEGG	Kyoto Encyclopedia of Genes and Genomes
OB	Oral bioavailability
DL	Drug-likeness
SRC	Proto-oncogene tyrosine-protein kinase Src
Akt1	RAC-alpha serine/threonine-protein kinase 1
CTNNB1	Catenin beta-1
EGFR	Epidermal growth factor receptor
ESR1	Estrogen receptor 1
BP	Biological process
CC	Cellular component
MF	Molecular function

Declarations

Author contributions: Conceptualization, Y.R., W.K. and X.H.; Data curation, X.H.; Formal analysis, Y.C. and W.D.; Funding acquisition, Y.L., X.Y., W.K. and X.H.; Investigation, Y.L., B.T. and W.D.; Methodology, Y.L. and W.D.; Project administration, W.D. and X.H.; Resources, W.P., Y. R. and X.H.; Software, B.T.; Supervision, X.H.; Validation, W.P.; Visualization, B.T.; Writing – original draft, Y. L. and X.H.; Writing – review & editing, H. U., X.Y. and X.H. All authors have read and agreed to the published version of the manuscript.

Funding: This research was funded by Special Fund for Science and Technology Development of Zhanjiang (2022A01003), Dongguan Science and Technology of Social Development Program (20231800939832), Natural Science Foundation of Guangdong Province of China (2022A1515011302, 2023A1515011116), Discipline construction project of Guangdong Medical University (4SG24002G), Key Research and Development Project of Huizhou, China (2023CZ010001), Talent Development Foundation of The First Dongguan Affiliated Hospital of Guangdong Medical University & Foundation of State Key

Laboratory of Pathogenesis, Prevention and Treatment of High Incidence Diseases in Central Asia (SKL-HIDCA-2024-GD1, SKL-HIDCA-2024-GD15), Student Innovation Research and Entrepreneurship Training of Guangdong Medical University (GDMU2022059, GDMU2022177).

Data availability statement: All the data supporting the results were shown in the paper, and can be obtained from the corresponding author.

Ethics approval and consent to participate

Not applicable.

Consent for publication

Not applicable.

Competing interests

The authors declare no competing interests.

References

1. Han B, Zheng R, Zeng H, Wang S, Sun K, Chen R, et al. Cancer incidence and mortality in China, 2022. J Natl Cancer Cent. 2024;4(1):47–53.
2. Sharma R, Abbasi-Kangevari M, Abd-Rabu R, Abidi H, Abu-Gharbieh E, Acuna JM, et al. Global, regional, and national burden of colorectal cancer and its risk factors, 1990–2019: a systematic analysis for the Global Burden of Disease Study 2019. Lancet Gastroenterol Hepatol. 2022;7(7):627–47.
3. Keum N, Giovannucci E. Global burden of colorectal cancer: emerging trends, risk factors and prevention strategies. Nat Rev Gastroenterol Hepatol. 2019;16(12):713–32.
4. Dariya B, Aliya S, Merchant N, Alam A, Nagaraju GP. Colorectal cancer biology, diagnosis, and therapeutic approaches. Crit Rev Oncog. 2020;25:71–94.
5. Macharia JM, Mwangi RW, Rozmann N, Zsolt K, Varjas T, Uchechukwu PO, et al. Medicinal plants with anti-colorectal cancer bioactive compounds: Potential game-changers in colorectal cancer management. Biomed Pharmacother. 2022;153:113383.
6. Dai W, Chen C, Feng H, Li G, Peng W, Liu X, et al. Protection of Ficus pandurata Hance against acute alcohol-induced liver damage in mice via suppressing oxidative stress, inflammation, and apoptosis. J Ethnopharmacol. 2021;275:114140.
7. Lv H, Zhang X, Chen X, Xie Z, Hu C, Wen C, et al. Phytochemical compositions and antioxidant and anti-inflammatory activities of crude extracts from Ficus pandurata H. (Moraceae). Evid Based Complement Alternat Med. 2013;2013:1–8.

8. Lv H, Hu C, Xie Z, Wang P, Chen X, Wen C. Purification, characterization and anti-tumor activity of a pectic-type polysaccharide isolated from Ficus pandurata H. Int J Biol Macromol. 2020;153:201–6.
9. Dai W, Zhan X, Peng W, Liu X, Peng W, Mei Q, et al. Ficus pandurata Hance inhibits ulcerative colitis and colitis-associated secondary liver damage of mice by enhancing antioxidation activity. Oxid Med Cell Longev. 2021;2021:1–16.
10. Danese S, Malesci A, Vetrano S. Colitis-associated cancer: the dark side of inflammatory bowel disease. Gut. 2011;60(12):1609–10.
11. Terzić J, Grivennikov S, Karin E, Karin M. Inflammation and colon cancer. Gastroenterology. 2010;138(6):2101–e145.
12. Zhi J, Yin L, Zhang Z, Lv Y, Wu F, Yang Y, et al. Network pharmacology-based analysis of Jin-Si-Wei on the treatment of Alzheimer's disease. J Ethnopharmacol. 2024;319:117291.
13. Lin H, Wang X, Liu M, Huang M, Shen Z, Feng J, et al. Exploring the treatment of COVID-19 with Yinqiao powder based on network pharmacology. Phytother Res. 2021;35(5):2651–64.
14. Lin Q, Ren L, Jian M, Xu P, Li J, Zheng P, et al. The mechanism of the premetastatic niche facilitating colorectal cancer liver metastasis generated from myeloid-derived suppressor cells induced by the S1PR1–STAT3 signaling pathway. Cell Death Dis. 2019;10(10):693.
15. Majid M, Nasir B, Zahra SS, Khan MR, Mirza B, Haq I-u. Ipomoea batatas L. Lam. ameliorates acute and chronic inflammations by suppressing inflammatory mediators, a comprehensive exploration using in vitro and in vivo models. BMC Complement Altern Med. 2018;18(1):216.
16. Yi W, Tong Z, Chuyue H, Fei L, Yang Z, Desong K, et al. Effect and mechanism of Banxia Xiexin decoction in colorectal cancer: A network pharmacology approach. Phytomedicine. 2024;123:155174.
17. Zou M, Zhang Y, Feng J, Tu H, Gui M, Wang Y, et al. Serum metabolomics analysis of biomarkers and metabolic pathways in patients with colorectal cancer associated with spleen-deficiency and qi-stagnation syndrome or damp-heat syndrome: a prospective cohort study. Front Oncol. 2023;13:1190706.
18. Huang L, Liu J, Jin Y, Qiu Y, Qin X, Wu S, et al. Niujiao Dihuang Jiedu decoction promotes SLC7A11 m5C methylation modification against ferroptosis in acute-on-chronic liver failure. Phytomedicine. 2024;122:155136.
19. Qu F, Li D, Zhang S, Zhang C, Shen A. The potential mechanism of qinghua quyu jianpi decoction in the treatment of ulcerative colitis based on network pharmacology and experimental validation. J Ethnopharmacol. 2023;310:116396.
20. Chen H, Zhang G, Peng Y, Wu Y, Han X, Xie L, et al. Danggui Shaoyao San protects cyclophosphamide-induced premature ovarian failure by inhibiting apoptosis and oxidative stress through the regulation of the SIRT1/p53 signaling pathway. J Ethnopharmacol. 2024;323:117718.
21. Rejhová A, Opattová A, Čumová A, Slíva D, Vodička P. Natural compounds and combination therapy in colorectal cancer treatment. Eur J Med Chem. 2018;144:582–94.

22. Dai W, Pang X, Peng W, Zhan X, Chen C, Zhao W, et al. Liver protection of a low-polarity fraction from Ficus pandurata Hance, prepared by supercritical CO2 fluid extraction, on CCl4-induced acute liver injury in mice via inhibiting apoptosis and ferroptosis mediated by strengthened antioxidation. Molecules. 2023;28(5):2078.
23. Lizcano JM, Göransson O, Toth R, Deak M, Morrice NA, Boudeau J, et al. LKB1 is a master kinase that activates 13 kinases of the AMPK subfamily, including MARK/PAR-1. EMBO J. 2004;23(4):833–43.
24. Gwinn DM, Shackelford DB, Egan DF, Mihaylova MM, Mery A, Vasquez DS, et al. AMPK phosphorylation of raptor mediates a metabolic checkpoint. Mol Cell. 2008;30(2):214–26.
25. Ken I, Zhu T, Guan K. TSC2 mediates cellular energy response to control cell growth and survival. Cell. 2003;115:577–90.
26. Cotter TG. Apoptosis and cancer: the genesis of a research field. Nat Rev Cancer. 2009;9(7):501–7.
27. Watson AJM. Apoptosis and colorectal cancer. Gut. 2004;53(11):1701–9.
28. Carneiro BA, El-Deiry WS. Targeting apoptosis in cancer therapy. Nat Rev Clin Oncol. 2020;17(7):395–417.

Table 1

Table 1 is available in the Supplementary Files section.

Figures

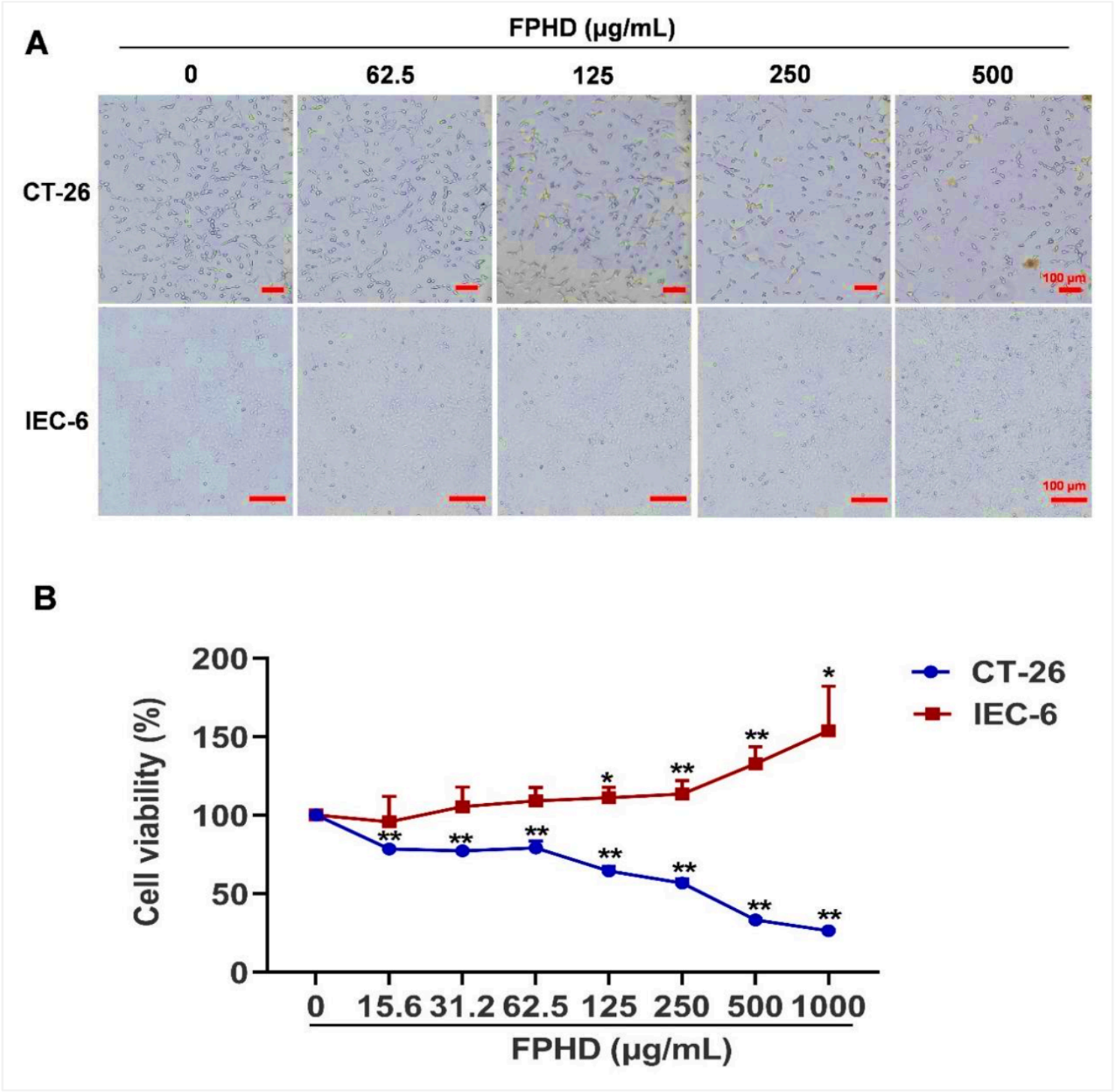

Figure 1

FPHD suppresses CT-26 cells growth in vitro. (A) Morphological observation of CT-26 (scale bar=100 μm) and IEC-6 cells (scale bar=100 μm) after FPHD treatment. (B) Viability of CT-26 and IEC-6 cells after FPHD treatment.

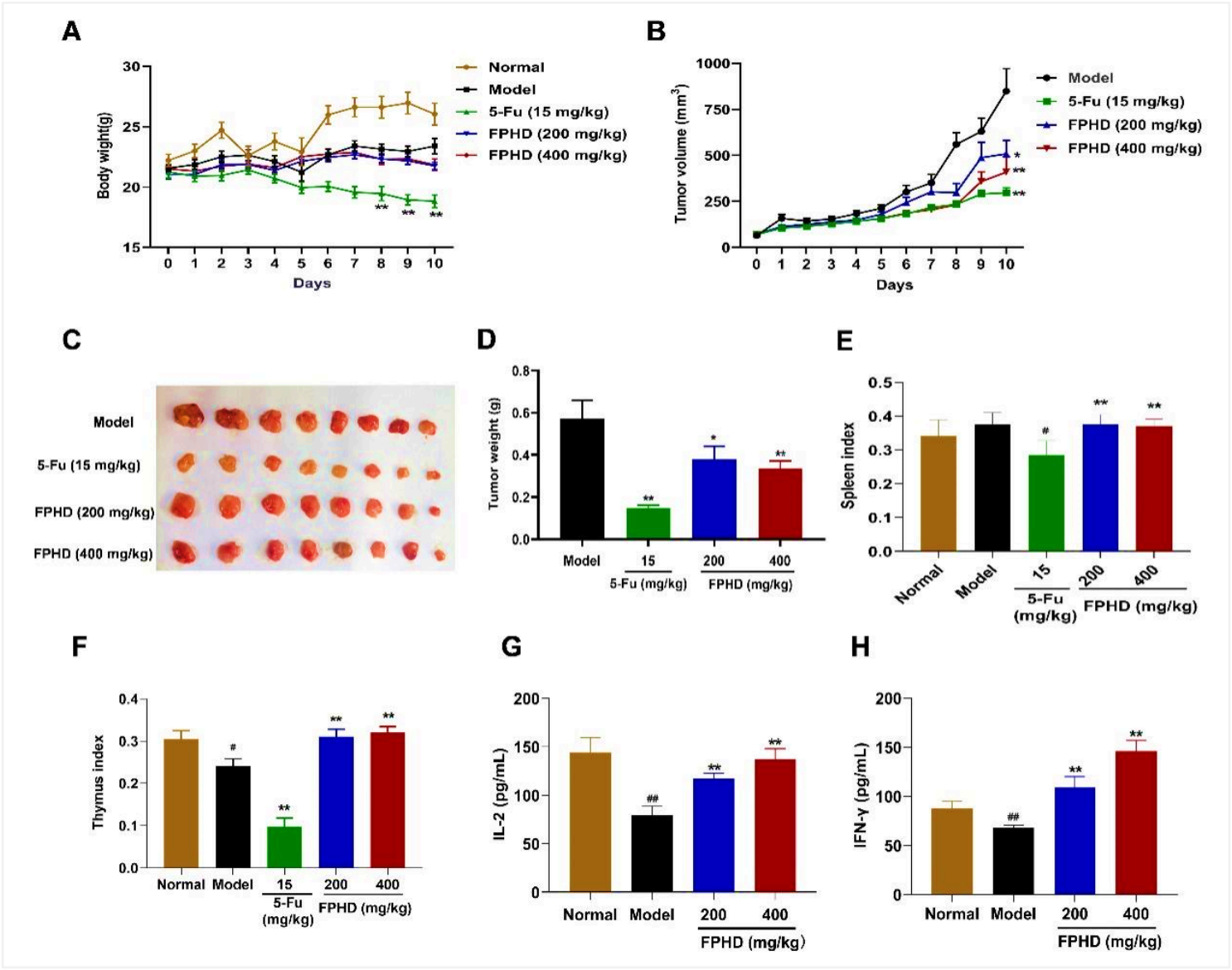

Figure 2

FPHD suppresses CT-26 cells growth *in vivo*. (A) Changes of mice body weight in the model, 5-FU, FPHD-treated (200, 400 mg/kg) groups. (B) The tumor volume of CT-26 tumor-bearing mice was measured for ten days after FPHD treatment. (C) Tumor photos of model, 5-FU, FPHD-treated (200, 400 mg/kg) groups. (D) Tumor weight in model, 5-FU, FPHD-treated (200, 400 mg/kg) groups. The index of spleen (E) and thymus (F) in model, 5-FU, FPHD (200, 400 mg/kg) groups. The serum cytokines of IL-2 (G) and IFN-γ (H) in the normal, model, and FPHD-treated (200, 400 mg/kg) groups. #$p < 0.05$, ##$p < 0.01$, compared with the normal group; *$p < 0.05$, **$p < 0.01$, compared with the model group.

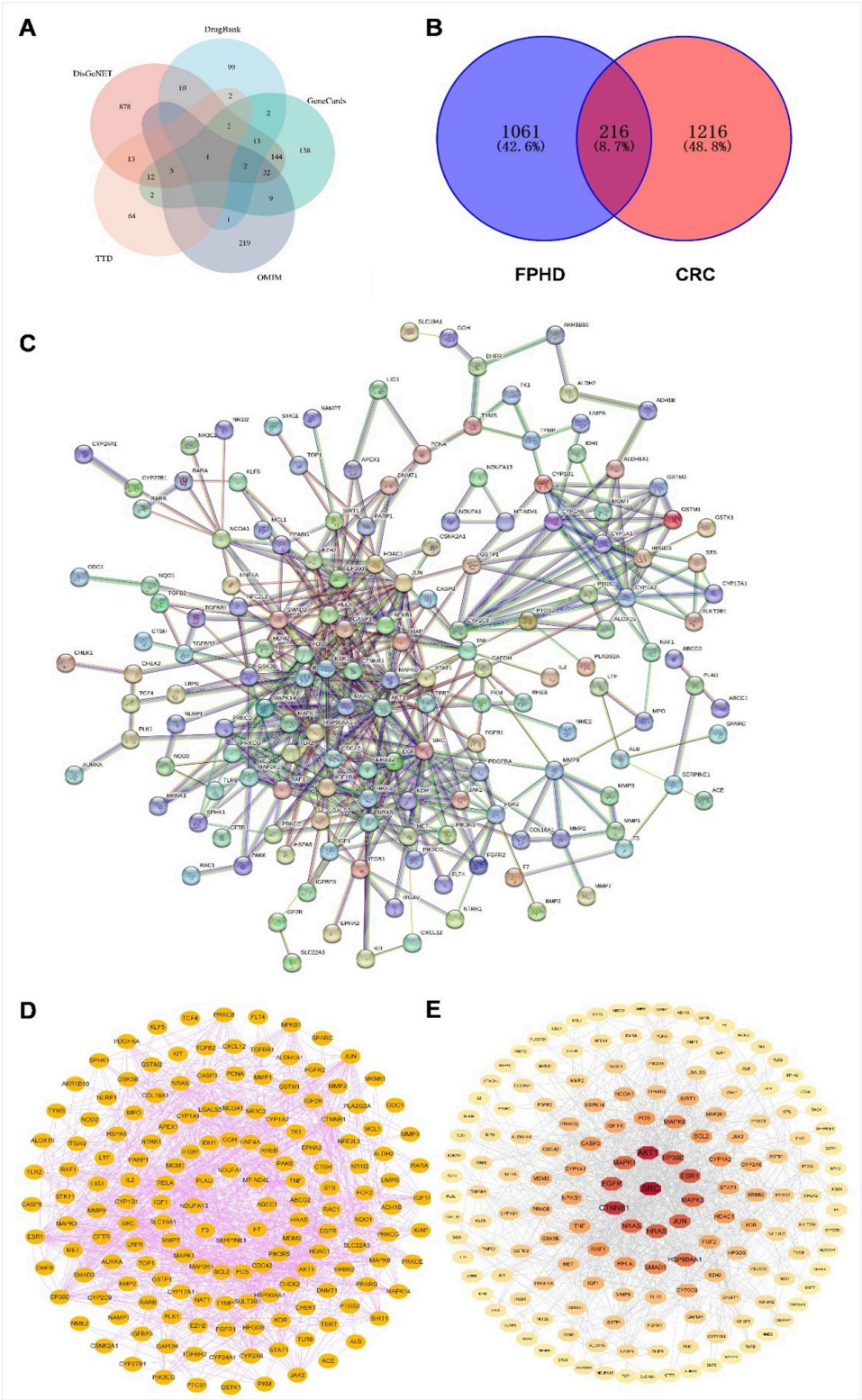

Figure 3

Network pharmacological analysis for FPHD against CRC. (A) Venn diagram of therapeutic targets obtained from four databases. (B) Venn diagram illustrating the intersecting targets between CRC and FPHD. (C, D) Protein-protein interaction (PPI) network analysis. (E) Target interaction network parameters analysis.

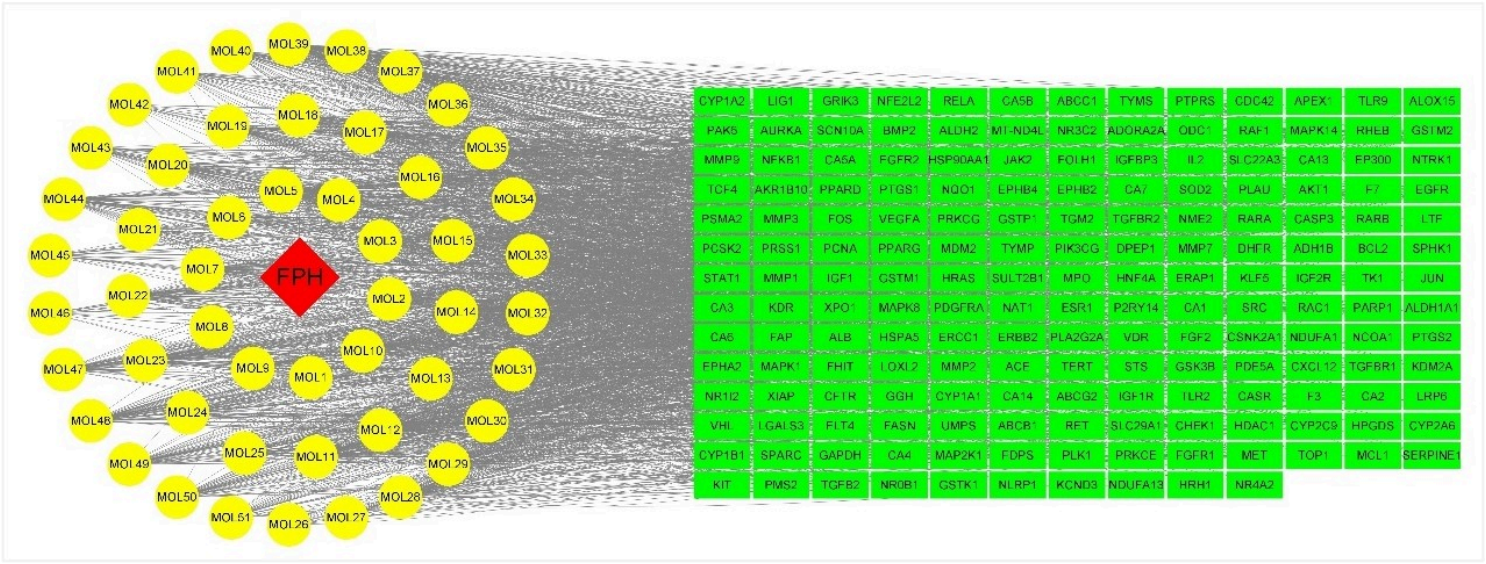

Figure 4

Herb-compound-pathway-target network. MOL1: Creatinine; MOL2: 2,3-Dihydro-5,7-dihydroxy- 2,8-dimethyl-6-(3-methyl-2- butenyl)-4H-1-benzopyran- 4-one; MOL3: gamma-Octalactone; MOL4: Histamine; MOL5: Sinapine; MOL6: Nicotinic acid; MOL7: Mimosine; MOL8: Nicotinamide; MOL9: Gentianaine; MOL10: Tuliposide B; MOL11: Cryptochlorogenic acid; MOL12: Verbenalin; MOL13: Tuberosine A; MOL14: Bavachin; MOL15: Quassimarin; MOL16: Piceatannol; MOL17: Succinic acid; MOL18: Polydatin; MOL19: Protocatechuic acid; MOL20: Canthoside B; MOL21: 4-Hydroxybenzoic acid; MOL22: Geniposide; MOL23: Justicidin B; MOL24: Daphentin; MOL25: Syringic acid; MOL26: Methyl(2,4-dihydroxy-3-formyl-6-methoxy)phenylketone; MOL27: p-Coumaric acid; MOL28: 7-Hydroxycoumarin; MOL29: Berberastine; MOL30: Methyl-5,7-dihydroxy- 2(Z)-octenoate; MOL31: Podolide; MOL32: Loliolide; MOL33: Icariside B9; MOL34: Miraxanthin III; MOL35: Bruceine E; MOL36: Angelol B; MOL37: Tagitinin F; MOL38: Erianin; MOL39: Dihydrocapsaicin; MOL40: Terpinyl acetate; MOL41: Santenone alcohol; MOL42: Gentianadine; MOL43: Menthyl acetate; MOL44: Aristolophenanlactone I; MOL45: Mesaconic acid; MOL46: Pyroracemic acid; MOL47: trans-Aconitic acid; MOL48: 5,6,7-Trimethoxycoumarin; MOL49: Sanleng acid; MOL50: 6-Gingerol; MOL51: Damascenine.

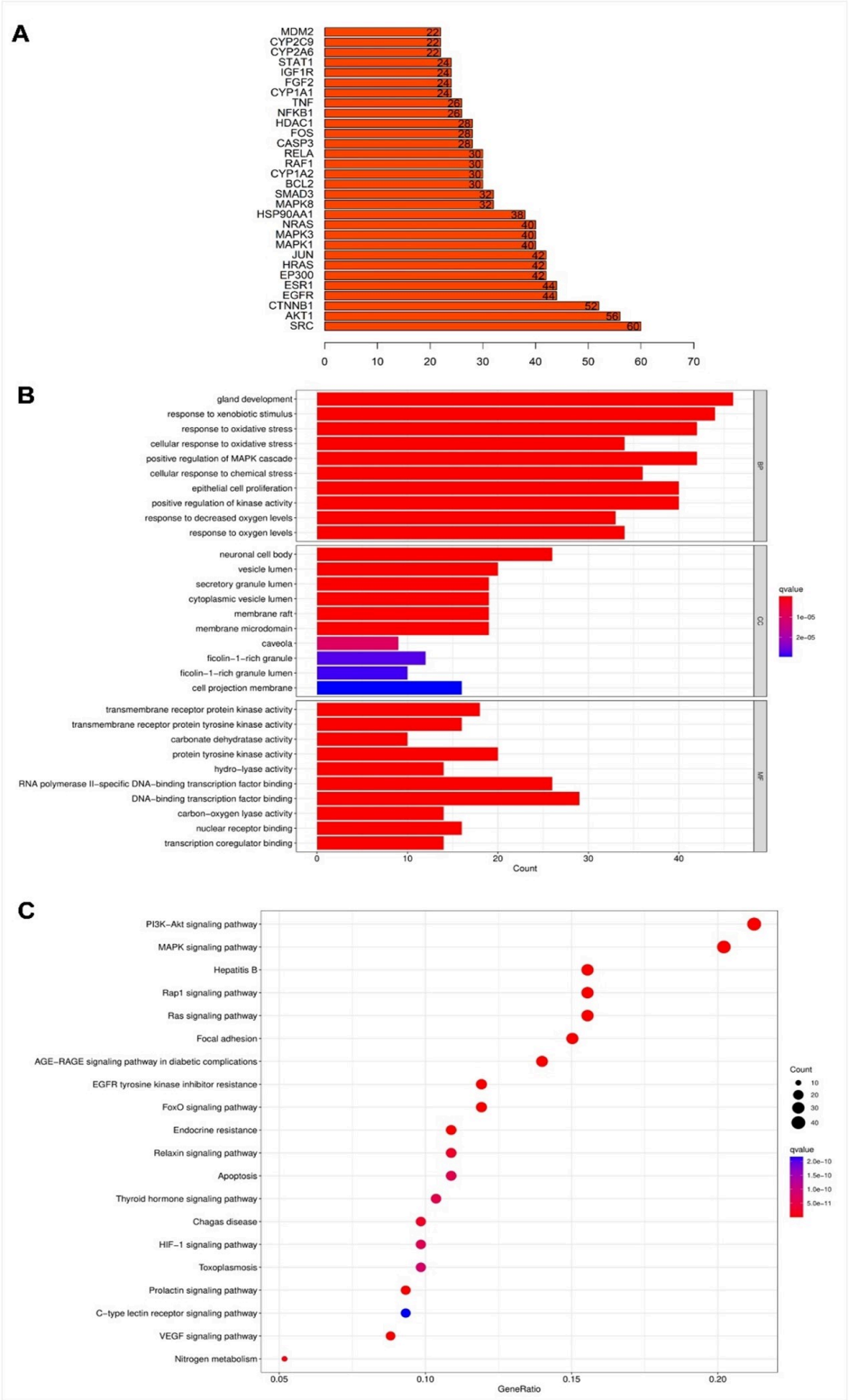

Figure 5

Characterization of key genes for FPHD against CRC. (A) The top 30 genes by degree value in the PPI network. (B) GO analysis for identified targets. (C) Pathway enrichment analysis using KEGG.

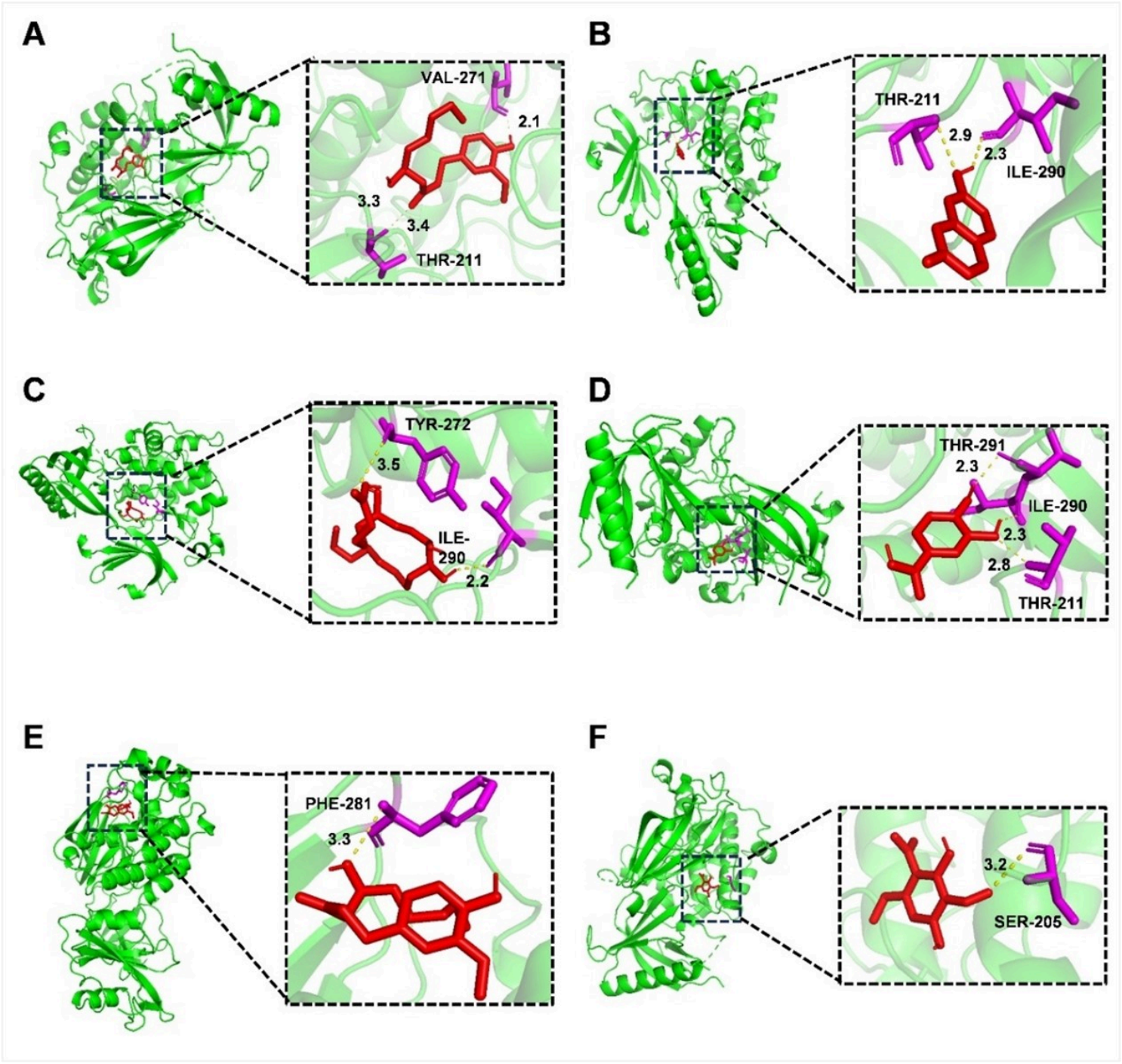

Figure 6

Molecular docking analysis. (A) Akt1 with 6-Gingerol. (B) Akt1 with 7-Hydroxycoumarin. (C) Akt1 with Sanleng acid. (D) Akt1 with Protocatechuic acid. (E) SRC with 6-Gingerol. (F) Akt1 with Methyl(2,4-dihydroxy-3-formyl-6- methoxy)phenylketone. The hydrogen bonds were indicated by dashed lines and the length was added around the lines.

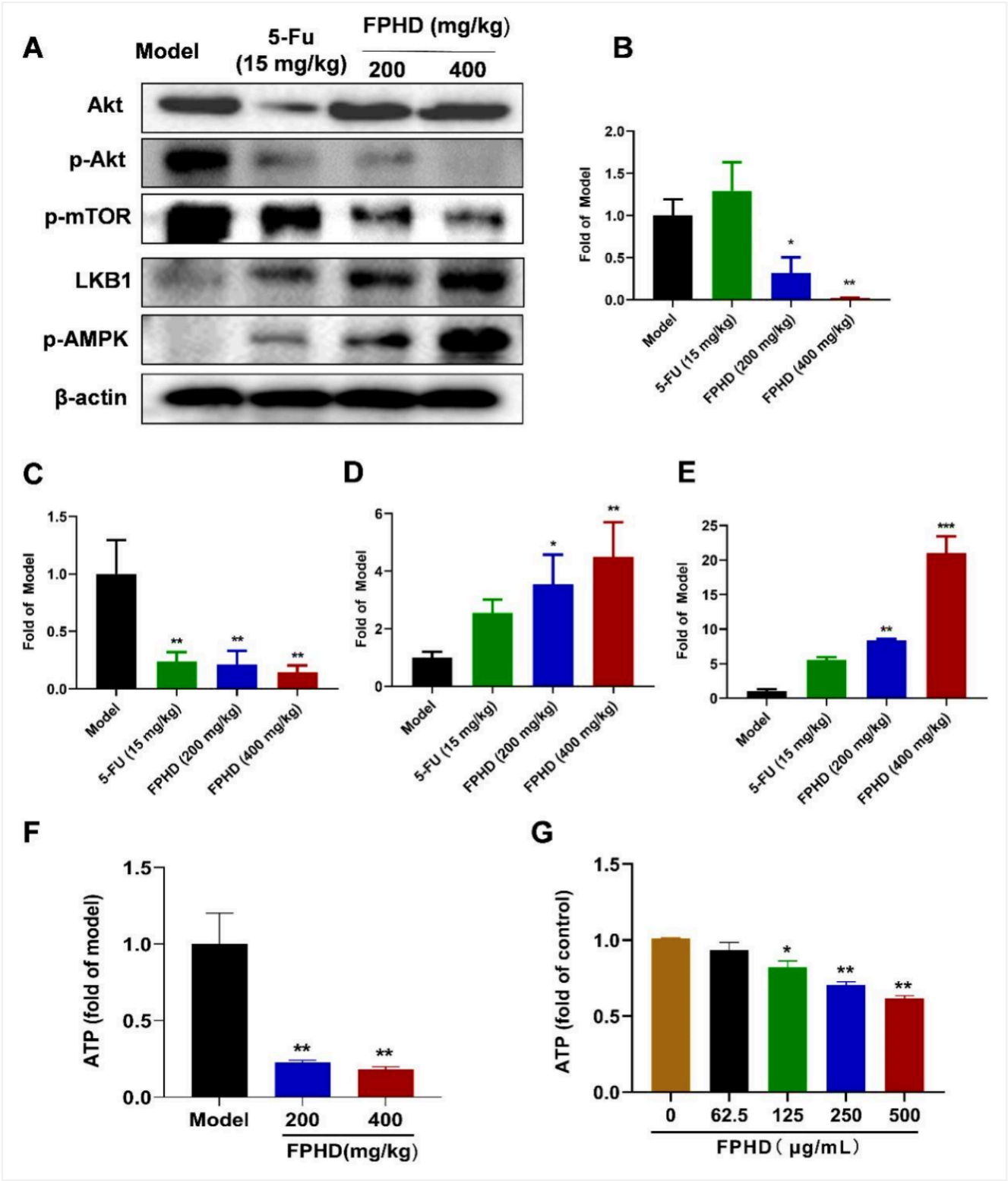

Figure 7

FPHD suppressed CRC growth via limiting energy production mediated by regulating the PI3K/Akt/mTOR signaling pathway. The protein expression of the PI3K/Akt/mTOR pathway was measured by Western Blot (A) and quantitative analysis for Akt/p-Akt (B), p-mTOR (C), LKB1 (D) and p-AMPK (E). The ATP levels in tumors (F) or cells (G) were determined via an ATP Assay kit. *$p < 0.05$, **$p < 0.01$, **$p < 0.001$, compared with model or control group.

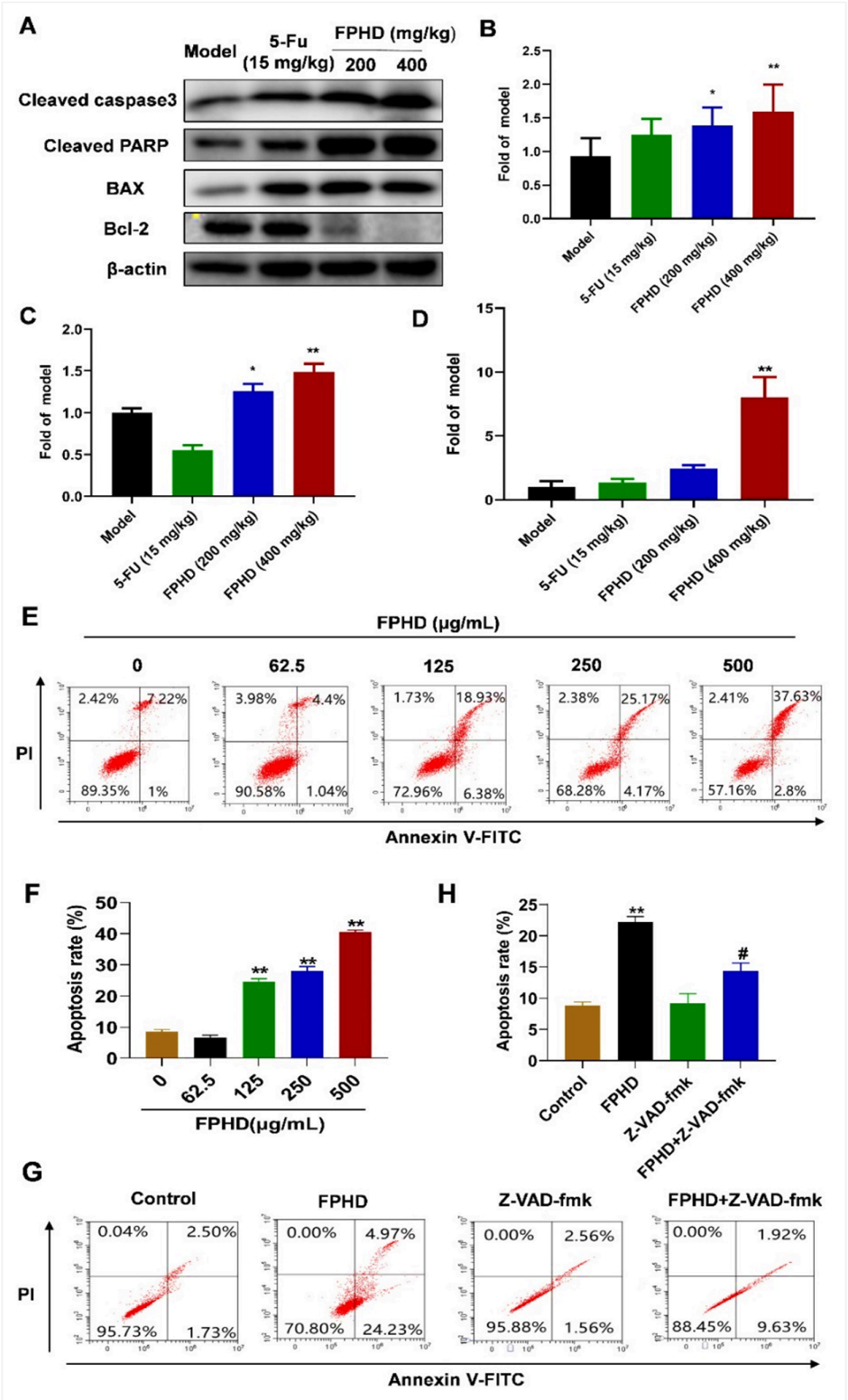

Figure 8

FPHD inhibited CRC growth via inducing apoptosis. (A-D) The effect of FPHD on apoptosis-related proteins in tumors. Mice bearing CT-26 tumors were treated with FPHD (200, 400 mg/kg) or 5-FU (15 mg/kg), and the levels of apoptosis-related proteins were detected by Western Blot (A). Quantitative analysis for cleaved caspase 3 (B), cleaved PARP (C), BAX/Bcl-2(D). (E-G) The effect of FPHD on cell apoptosis (E). Quantitative analysis for apoptosis rates (F). Cells were pretreated with a pan-caspase

inhibitor Z-VAD-fmk and the apoptotic cells were detected (G, H). *p< 0.05, **p < 0.01, compared with the model or control group. #p< 0.05, compared with FPHD only.

Supplementary Files

This is a list of supplementary files associated with this preprint. Click to download.

- GA.png
- Table1.docx
- RawdataforWesternBlot20250507.pdf